Dalton Transactions

PAPER

View Article Online
View Journal | View Issue

Cite this: *Dalton Trans.*, 2019, **48**, 1993

Nucleobase-mediated synthesis of nitrogen-doped carbon nanozymes as efficient peroxidase mimics†

Shichao Lin,[a] Yihong Zhang,[a] Wen Cao,[a] Xiaoyu Wang,[a] Li Qin,[a] Min Zhou[a] and Hui Wei *[a,b]

Received 12th November 2018,
Accepted 4th January 2019

DOI: 10.1039/c8dt04499f

rsc.li/dalton

Carbon nanozymes are catalytic carbon nanomaterials with intrinsic enzyme-like activities. They are advantageous over their natural counterparts in terms of higher stability, lower preparation cost, and better robustness. However, the peroxidase-like activities of the most developed carbon nanozymes were moderate due to the imperfection of active centers and limited tuning strategies. Herein, we designed a novel class of efficient peroxidase-mimicking carbon nanozymes with nitrogen atom doping. The N-doped carbon nanozymes were facilely synthesized by direct pyrolysis of different nucleobases at controlled temperatures without other treatments. A high ratio of nitrogen atoms was doped into the carbon skeleton. For example, 8.77 wt% of N remained in the guanine-derived carbon nanozyme with a pyrolysis temperature of 900 °C. The dominant graphitic N species greatly boosted the peroxidase-like activities of nucleobase-derived carbon nanozymes. Moreover, nucleobases are cheap, abundant, and environmentally friendly. We have demonstrated that nitrogen-rich nucleobases are ideal starting materials for the large-scale and cost-effective synthesis of N-doped carbon nanozymes. The carefully designed N-doped carbon nanozymes with superior activities were further used to construct effective biosensors for bioactive molecules (*i.e.*, H_2O_2 and glucose). Highly sensitive and selective detection of H_2O_2 and glucose was achieved using the N-doped carbon nanozymes as efficient peroxidase mimics. This study offers an economical and sustainable approach for the scalable preparation of N-doped carbon nanozymes and creates a new path for the rational design of efficient peroxidase-mimicking carbon nanozymes by heteroatom doping.

Introduction

Natural enzymes are exquisite biocatalysts with extraordinary activity and selectivity.[1] However, the practical applications of enzymes are inevitably limited by their intrinsic drawbacks such as poor stability, sensitivity towards environmental conditions, and high cost of preparation. In the past decades, intensive efforts have been devoted to the research on alternatives to enzymes, called "artificial enzymes".[2,3] Among them, nanomaterials with enzyme-like characteristics (nanozymes) are attractive due to their low cost of preparation, high stability under various conditions, multi-functionalities, and tunable catalytic activities.[4–17]

In 2010, Qu *et al.* demonstrated that graphene oxide (GO) nanosheets exhibited intrinsic peroxidase-like activity,[18] which has ignited great research interest in the exploration of peroxidase-mimicking carbon nanozymes.[19] GO, carbon dots, carbon nanotubes, and their derivatives have been investigated as peroxidase mimics.[19–22] Comprehensive insights into the catalytic mechanism of carbon nanozymes showed that surface oxygen species were the active sites of the peroxidase-mimicking carbon nanozymes.[23] However, the activation of a reaction substrate (*i.e.*, H_2O_2) was impeded by the high adsorption energy barrier.[24] As a result, the intrinsic peroxidase-like activities of the reported carbon nanozymes are moderate when compared with other nanozymes or natural horseradish peroxidase (HRP).[25,26] To date, it still remains a grand challenge to enhance the intrinsic peroxidase-like activity of carbon nanozymes.[19]

To address this challenge, we have recently reported that the incorporation of the heteroatom N into a carbon skeleton greatly boosted the peroxidase-like activities of carbon nanozymes with exceptional specificity.[27] Nevertheless, the N-doped

[a]*Department of Biomedical Engineering, College of Engineering and Applied Sciences, Collaborative Innovation Center of Chemistry for Life Sciences, Nanjing National Laboratory of Microstructures, Nanjing University, Nanjing, Jiangsu 210093, China*
[b]*State Key Laboratory of Analytical Chemistry for Life Science and State Key Laboratory of Coordination Chemistry, School of Chemistry and Chemical Engineering, Nanjing University, Nanjing, Jiangsu 210093, China.*
E-mail: weihui@nju.edu.cn; http://weilab.nju.edu.cn; Fax: +86-25-83594648; Tel: +86-25-83593272

†Electronic supplementary information (ESI) available. See DOI: 10.1039/c8dt04499f

carbon nanozymes were prepared through complicated procedures or even with silica templates. In addition, the high cost of preparation, limited yield, and ammonia waste made them challenging for practical applications. Therefore, it is highly desired to exploit greener synthetic approaches to obtain large-scale and cheap N-doped carbon nanomaterials with high nitrogen contents as efficient peroxidase mimics.[28–31]

Nucleobases are nitrogen-rich biological compounds that form nucleosides and nucleotides.[1] There are five natural nucleobases, including adenine (A), cytosine (C), guanine (G), thymine (T) and uracil (U).[1] Interestingly, different from nucleosides and nucleotides, nucleobases are cheaper and readily available in large quantities. Therefore, they have been widely used as building blocks to construct various functional nanomaterials.[32–36] We reason that the rich and diverse proportion of nitrogen in nucleobases would make them ideal to prepare N-doped carbon nanomaterials with high nitrogen contents and tunable catalytic activities from nucleobases.

Herein, we demonstrate a novel, cost-effective, and readily scalable strategy for the preparation of N-doped carbon nanozymes. By direct pyrolysis of different nucleobases at controlled temperatures, N-doped carbon nanozymes with tunable peroxidase-like activity were successfully obtained without complex procedures or producing undesired waste. Interestingly, carbon nanozymes derived from guanine at 900 °C, denoted as GNC900, stood out with the highest peroxidase-like activity among the nucleobase-derived N-doped carbon nanozymes. The remarkable peroxidase-like activity of GNC900 was investigated by enzyme kinetics studies. To demonstrate the effectiveness of the N doping strategy, colorimetric detection of bioactive molecules (*i.e.*, H_2O_2 and glucose) based on GNC900 was developed with excellent sensitivity and selectivity.

Results and discussion

Synthesis of nitrogen-doped carbon nanozymes

Scheme 1 depicts the facile, scalable, and cost-effective synthesis of N-doped carbon nanozymes from nucleobases. Direct pyrolysis of nitrogen-rich nucleobases at controlled temperatures opened up a new path to the synthesis of N-doped carbon nanozymes. Recent advancements in the typical N-doped carbon nanomaterial synthesis are summarized in Table S1.† Detailed comparison of the recent reports with the current work validated the advantages of our approach in the N-doped carbon nanomaterial preparation. Most of the reported methods suffer from the use of additional precursors and templates, complicated procedures, high cost, limited yields or undesired waste production. In contrast, the proposed nucleobase-based approach in this work offered a new solution to the greener preparation of N-doped carbon nanomaterials for practical applications.

The obtained black powder was readily used as highly efficient peroxidase mimics without further treatments. The oxidation of peroxidase substrates (*i.e.*, TMB) by H_2O_2 was greatly accelerated in the presence of N-doped carbon nanozymes. Among the obtained N-doped carbon nanozymes, the one derived from guanine at 900 °C (GNC900) stood out with the highest peroxidase-like activity (*vide infra*). Thus, GNC900 was selected as a representative example for the study of the newly developed N-doped carbon nanozymes.

The morphology of the as-synthesized GNC900 was revealed by SEM and TEM characterization. Interestingly, GNC900 has a graphene-like structure with typical wrinkles (Fig. 1a and b). The XRD pattern exhibited a distinct characteristic peak at about 25.8°, which was ascribed to the (002) plane of graphitic carbon (Fig. 1c). The graphitic carbon structure from a high temperature pyrolysis was further confirmed by high resolution transmission electron microscopy (HRTEM). Clear fringes indicated the formation of the graphitic carbon structure (Fig. S1†). The successful doping of N atoms into the carbon

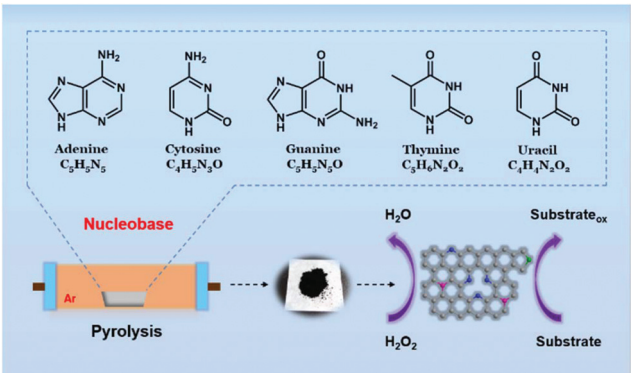

Scheme 1 Schematic illustration of the synthesis of N-doped carbon nanozymes from nucleobases as efficient peroxidase mimics.

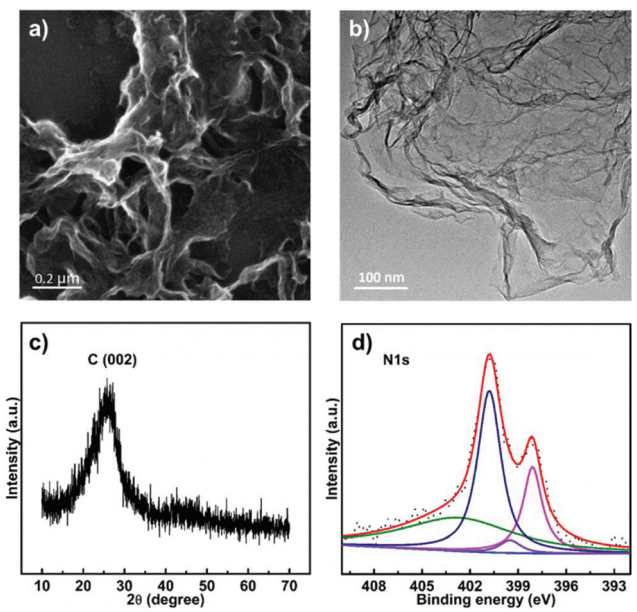

Fig. 1 Representative (a) SEM and (b) TEM images of GNC900. (c) XRD pattern of GNC900. (d) High resolution XPS spectra of N 1s for GNC900.

skeleton was validated by using XPS spectra (Fig. S2†). The obtained GNC900 showed a N content as high as 8.77 wt% (Table S2†). Other potential metallic impurities were ruled out by thermal gravimetric analysis (TGA) characterization. GNC900 was decomposed thoroughly at high temperature without leaving any metal oxide (Fig. S3†). Generally, unstable C and N fragments were released during the pyrolysis at high temperature (*i.e.*, 900 °C), leading to a low doping ratio of N in carbon. Interestingly, GNC900 maintained a high N portion due to the unique nature of N-rich guanine. In our previous density functional theory (DFT) calculations,[27] the incorporation of graphitic N into a carbon scaffold greatly reduced the adsorption energy of H_2O_2. The favorable adsorption of H_2O_2 onto the active sites around graphitic N led to lower reaction barriers and thus remarkably enhanced the peroxidase-like activity of N-doped carbon nanozymes. The N bonding configuration in GNC900 was also investigated by using the high resolution XPS spectra of N 1s (Fig. 1d). Dominant graphitic N species (39.88 at%) in GNC900 was beneficial for the high peroxidase-mimicking activity (Table S3†).

Peroxidase-like activity of N-doped carbon nanozymes

The intrinsic peroxidase-like activity of GNC900 was first evaluated by the oxidation of the typical chromogenic substrate TMB in the presence of H_2O_2. The oxidized TMB (TMB_{ox}) exhibited a deep blue color with two distinct peaks at 370 nm and 652 nm. As shown in Fig. 2a, a deep blue color and strong absorption peaks at 370 nm and 652 nm were observed in the presence of TMB, H_2O_2, and GNC900. Negligible color changes were observed in other control groups. This clearly indicated that the oxidation of TMB by H_2O_2 was greatly accelerated by the peroxidase-mimicking GNC900. Two other chromogenic substrates, OPD and ABTS, were also investigated to further confirm the peroxidase-like activity of GNC900. GNC900 successfully catalyzed the oxidation of OPD and ABTS by H_2O_2 to their yellow and green oxidized products, respectively (Fig. 2b). Together, the colorimetric reactions demonstrated that the N-doped GNC900 exhibited intrinsic peroxidase-like activity.

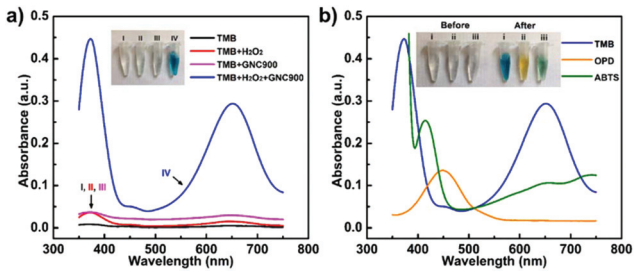

Fig. 2 (a) UV-visible absorption spectra of (I) TMB, (II) TMB + H_2O_2, (III) TMB + GNC900, and (IV) TMB + H_2O_2 + GNC900. Inset: Corresponding digital photograph of the reaction systems. (b) UV-visible absorption spectra of different chromogenic substrates oxidized by H_2O_2 in the presence of GNC900. Inset: Digital photographs of the reaction systems showing the color changes of (i) TMB, (ii) OPD, (iii) and ABTS before and after the GNC900 catalyzed oxidation, respectively.

The five nucleobases, including adenine (A), cytosine (C), guanine (G), thymine (T), and uracil (U), have distinct skeletal structures. Therefore, we expected that their carbonized products would exhibit different peroxidase-like activities. Kinetic curves of TMB_{ox} were recorded at 652 nm to monitor the catalytic oxidation of TMB with H_2O_2 in the presence of N-doped carbon nanozymes. A larger absorbance change in a certain time period (*i.e.*, 100 s) indicated a higher peroxidase-like activity of N-doped carbon nanozymes. At the same pyrolysis temperature (*i.e.*, 900 °C), the guanine derived N-doped carbon nanozyme (GNC900) showed the highest catalytic efficiency when compared with other nucleobase derived N-doped carbon nanozymes (Fig. 3a and c). Moreover, the peroxidase-like activity of guanine derived N-doped carbon nanozymes increased with the pyrolysis temperature (Fig. 3b and d). Among the nucleobase derived N-doped carbon nanozymes, GNC900 exhibited an overwhelmed peroxidase-mimicking activity. Therefore, GNC900 was selected as a representative of nucleobase derived N-doped carbon nanozymes for further investigations and applications.

The activities of natural peroxidases (*e.g.*, HRP) are dependent on the substrate concentration and reaction conditions. Similarly, the peroxidase-like activity of GNC900 was influenced by the substrate concentration, catalyst concentration, reaction pH, and temperature. The reaction rate increased with increasing concentration of H_2O_2 (Fig. 4a) or GNC900 (Fig. 4b). Moreover, the peroxidase-like activity of GNC900 was pH-dependent with the optimal activity at pH 4.5 (Fig. 4c), which was very close to natural HRP. Interestingly, the activity of GNC900 was increased even higher at higher reaction tempera-

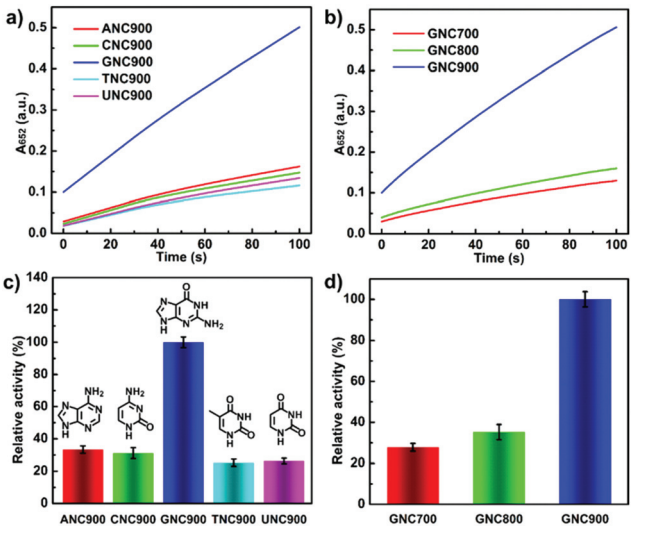

Fig. 3 Kinetic curves of the absorbance at 652 nm for monitoring the catalytic oxidation of TMB with H_2O_2 in the presence of N-doped carbon nanozymes derived from (a) different nucleobases at 900 °C or (b) guanine at different pyrolysis temperatures. (c) Comparison of the peroxidase-like activity of different nucleobases derived N-doped carbon nanozymes. (d) Comparison of the peroxidase-like activity of guanine derived carbon nanozymes at different pyrolysis temperatures. Error bars represent at least three independent measurements.

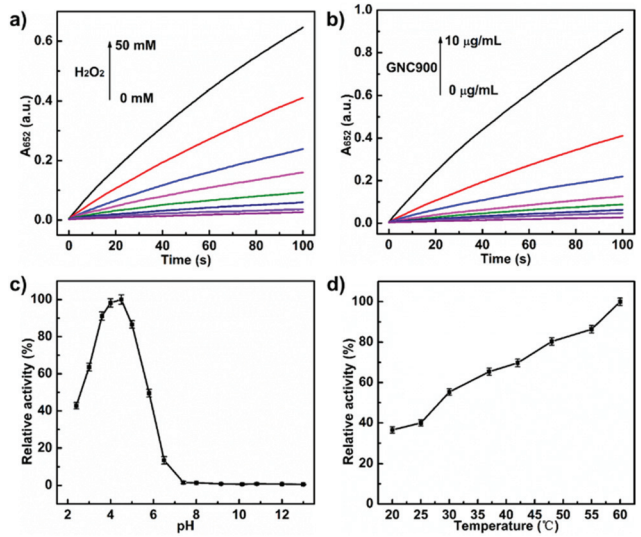

Fig. 4 Time-dependent absorption changes at 652 nm in the absence or presence of different concentrations of (a) H_2O_2 and (b) GNC900. (c) pH and (d) temperature dependent peroxidase-like activity of GNC900. Error bars represent at least three independent measurements.

tures (Fig. 4d). Since most of the natural enzymes are deactivated at a relatively high temperature, the positive correlation to reaction temperature of GNC activity was promising for practical applications (*i.e.*, in harsh environments).

To further investigate and quantify the peroxidase-like activity of GNC900, the apparent steady-state kinetics assays were carried out. Within the suitable range of TMB and H_2O_2 concentrations, the typical Michaelis–Menten curves were obtained (Fig. 5a and b). The apparent Michaelis–Menten parameters were calculated by fitting the Lineweaver–Burk equation in double reciprocal plots (Fig. 5c and d). The two key parameters, maximal reaction velocity (V_{max}) and Michaelis constant (K_m), were obtained (Table S4†). V_{max} represented the maximum initial velocity while K_m represented the affinity of the catalyst toward its substrate. GNC900 had similar affinities towards TMB and H_2O_2 when compared with HRP. It was noteworthy that GNC900 exhibited about one order higher value of V_{max} than HRP and other typical peroxidase-mimicking nanozymes (*e.g.*, the state-of-the-art GO-COOH) (Table S4†). This demonstrated the excellent peroxidase-like activity of the currently developed N-doped carbon nanozymes.

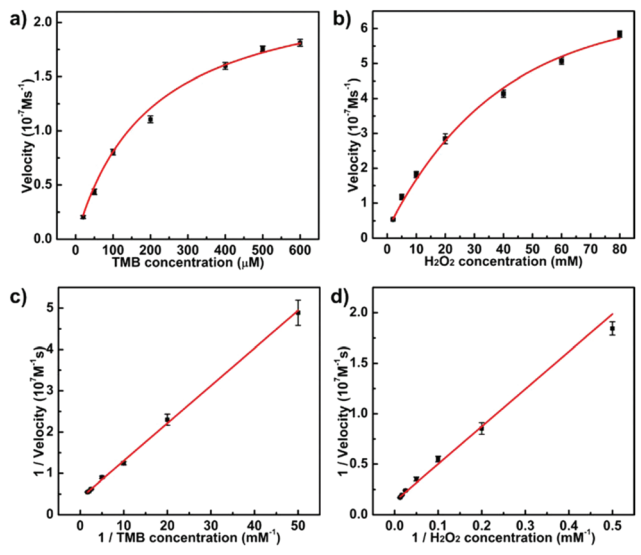

Fig. 5 Steady-state kinetics assays of GNC900 catalyzed oxidation of TMB by H_2O_2. Error bars represent at least three independent measurements.

Detection of H_2O_2 and glucose by N-doped carbon nanozymes

On the basis of the high performance of peroxidase-mimicking N-doped carbon nanozymes, colorimetric detection of biomedically important molecules was carried out for further applications. Due to the dependence of the peroxidase-like activity of GNC900 on H_2O_2, colorimetric detection of H_2O_2 was achieved by monitoring the absorption profiles of TMB (Fig. 6a). A dose-dependent curve for H_2O_2 detection was obtained with a linear range from 0.25 μM to 20 μM (Fig. 6b and c). The well-correlated plot indicated a detection limit of 115.5 nM H_2O_2 (Fig. 6d).

A cascade reaction combining glucose oxidase (GOx) and peroxidase-mimicking GNC900 was further developed for the detection of glucose (Fig. 7a). Aerobic oxidation of glucose was first catalyzed by GOx to produce H_2O_2. Then TMB was oxidized by the resultant H_2O_2 in the presence of GNC900. Thus, the detection of the concentration of glucose was easily achieved by monitoring the absorbance of blue colored TMB_{ox} (Fig. 7b). A dose-dependent curve of the absorbance at 652 nm

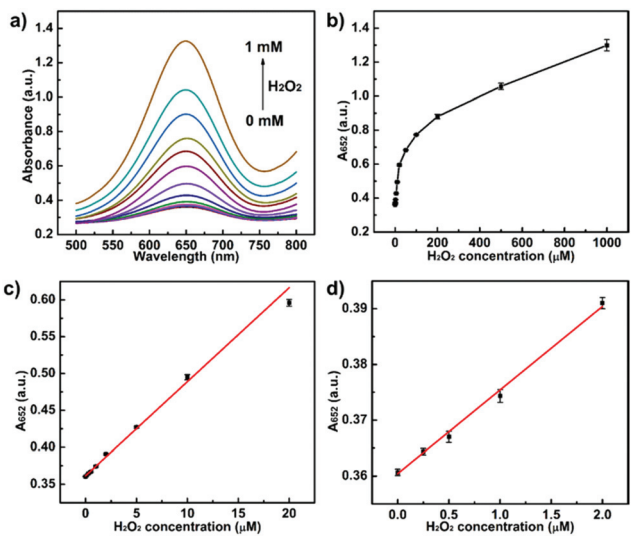

Fig. 6 (a) Typical absorption profiles of TMB in the presence of different concentrations of H_2O_2. (b) A dose dependent curve for H_2O_2 detection. (c) Linear calibration plot of H_2O_2 detection in the range from 0.25 μM to 20 μM. (d) Linear calibration plot of H_2O_2 detection showing a detection limit of 115.5 nM. Error bars represent at least three independent measurements.

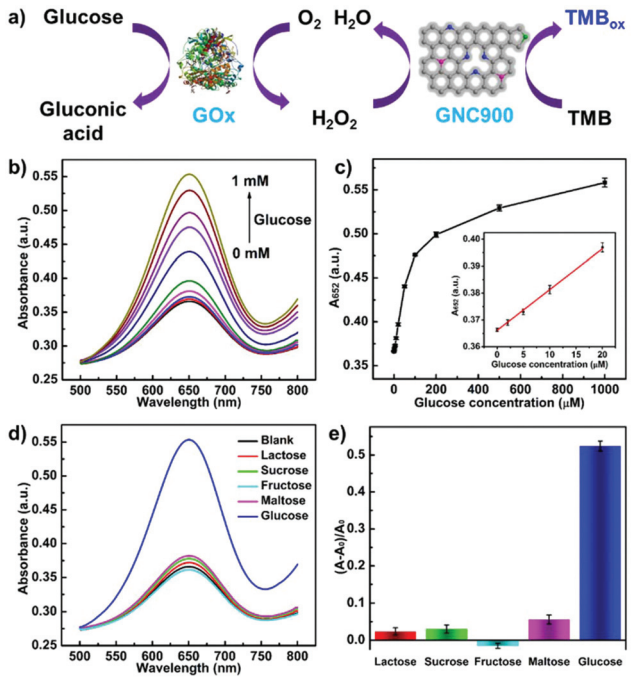

Fig. 7 (a) Schematic illustration of the glucose detection by GOx and GNC900 catalyzed cascade reactions (PDB code of GOx: 1CF3). (b) Typical absorption profiles of TMB in the presence of different concentrations of glucose. (c) A dose-dependent curve for glucose detection by GOx and GNC900 catalyzed cascade reactions. Inset: Linear calibration plot showing a detection limit of 1.14 μM. (d) Typical absorption profiles of TMB in the presence of 5 mM lactose, 5 mM sucrose, 5 mM fructose, 5 mM maltose, and 1 mM glucose. (e) Selective colorimetric detection of glucose. A and A_0 are the absorbances in the presence and absence of glucose or its analogues, respectively. Error bars represent at least three independent measurements.

for glucose detection was obtained with a linear range from 2 μM to 50 μM (Fig. S4†). The inset in Fig. 7c shows a linear calibration plot at a low concentration of glucose and a detection limit of 1.14 μM was achieved. The detection of glucose by representative carbon nanozymes based on their intrinsic peroxidase-like activity was compared with GNC900 in this work (Table S5†). Due to the superior peroxidase-like activity of GNC900, less catalyst and reaction time were required to fulfill the sensitive detection of glucose. To evaluate the selectivity of the established cascade reaction, controlled experiments were carried out with glucose analogues including lactose, sucrose, fructose, and maltose (Fig. 7d). Potentially interfering glucose analogues with a concentration of 5 mM led to negligible absorbance changes when compared with 1 mM glucose (Fig. 7e). Therefore, the cascade reaction combining GOx and peroxidase-mimicking GNC900 was capable of glucose detection with high activity and selectivity.

Conclusions

In conclusion, we reported a nucleobase-mediated strategy to synthesize N-doped carbon nanozymes, which was not only scalable and cost-effective but also environment friendly. It was noteworthy that nucleobases were the only source of carbon and nitrogen elements. High contents of N were doped into the carbon skeleton due to the unique nature of nucleobases. By direct pyrolysis of different nucleobases at controlled temperatures, a series of N-doped carbon nanozymes were obtained. Among them, GNC900 exhibited the highest peroxidase-like activity. The presence of abundant graphitic N in GNC900 was responsible for the superior peroxidase-mimicking ability. Moreover, GNC900 showed a H_2O_2-dependent peroxidase-like activity, which was adopted as an effective strategy for the sensitive detection of H_2O_2. When GOx was combined with GNC900 to fulfill a cascade reaction, glucose was successfully detected with high sensitivity and selectivity.

Experimental

Chemicals and materials

Adenine (99.5%), cytosine (98%), guanine (99%), thymine (99%), uracil (99%), 3,3′,5,5′-tetramethylbenzidine (TMB), 2,2′-azino-bis(3-ethylbenzothiazoline-6-sulphonic acid) (ABTS), *o*-phenylenediamine (OPD), and glucose oxidase (GOx from *Aspergillus niger*, >180 units per mg) were purchased from Aladdin Chemical Reagent Co., Ltd. Other chemicals were of at least analytical reagent grade. All the chemicals were used as received without further purification. All aqueous solutions throughout the experiments were prepared with deionized water (18.2 MΩ cm, Millipore).

Instrumentation

Scanning electron microscopy (SEM) was performed using a Zeiss Ultra 55 microscope (Zeiss, Germany). Transmission electron microscopy (TEM) images were obtained on a Tecnai F20 microscope (FEI, USA) at an acceleration voltage of 200 kV. Powder X-ray diffraction (XRD) data were obtained at room temperature on a Rigaku Ultima diffractometer (Rigaku, Japan) by using Cu Kα radiation. X-ray photoelectron spectroscopy (XPS) spectra were obtained on a PHI 5000 VersaProbe XPS microscope (UlVAC-PHI, Japan). UV-visible absorption spectra were recorded using a UV-visible spectrophotometer (TU-1900, Beijing Purkinje General Instrument Co. Ltd, China). Thermogravimetric analysis was carried out using a NETZSCH STA 409 PC/PG analyzer (NETZSCH, Germany) at a heating rate of 10 °C min^{-1}.

Synthesis of N-doped carbon nanozymes

N-Doped carbon nanozymes were obtained by direct pyrolysis of different nucleobases at controlled temperatures. In a typical synthesis, 1 g of nucleobase (A, C, G, T, and U) powder was transferred into a ceramic boat and placed in a tube furnace under a constant flow of argon gas. The nucleobase powder was heated to a desired temperature (T_{em}) at a ramping rate of 2 °C min^{-1} and kept for 3 h. After cooling down to room temperature, the black powder was collected as N-doped carbon nanozymes without further treatment. The

samples were denoted as XNCTem (X = A, C, G, T, and U; T_{em} = 700, 800, and 900 °C).

Peroxidase-like activity measurement

The peroxidase-like activity of N-doped carbon nanozymes was assessed as follows. N-doped carbon nanozyme XNCTem was added into 0.2 M NaOAc–HOAc buffer (pH 4.5) containing TMB and H_2O_2. The final concentrations of XNCTem, TMB, and H_2O_2 were 5 μg mL^{-1}, 625 μM, and 25 mM, respectively. The mixture was used for the UV-visible absorption spectra measurement.

Colorimetric detection of H_2O_2 and glucose using GNC900 as a peroxidase mimic

H_2O_2 detection was carried out as follows. Typically, 50 μL of GNC900 stock solution (200 μg mL^{-1}) and 32 μL of TMB stock solution (25 mM) were added into 0.2 M NaOAc–HOAc buffer (pH 4.5). The volume of the mixture was adjusted to 900 μL before adding 100 μL of H_2O_2 with various concentrations. The mixed solution was incubated at 37 °C for 20 min and then subjected to UV-visible absorption spectra measurement.

Glucose detection was carried out as follows. 100 μL of GOx (1 mg mL^{-1}) and 100 μL of glucose with various concentrations in 0.2 M phosphate buffer (pH 7.0) were incubated at 37 °C for 30 min. 50 μL GNC900 stock solution (200 μg mL^{-1}) and 32 μL TMB stock solution (25 mM) were added before adjusting the volume of the reaction solution to 1 mL. The mixed solution was incubated at 37 °C for 20 min and then subjected to UV-visible absorption spectra measurement.

Conflicts of interest

H. W. and S. L. are co-authors on patent applications.

Acknowledgements

This work was supported by the National Natural Science Foundation of China (21722503 and 21874067), 973 Program (2015CB659400), PAPD Program, Shuangchuang Program of Jiangsu Province, Open Funds of the State Key Laboratory of Analytical Chemistry for Life Science (SKLACLS1704), Open Funds of the State Key Laboratory of Coordination Chemistry (SKLCC1819), Fundamental Research Funds for the Central Universities (021314380103), and Thousand Talents Program for Young Researchers.

Notes and references

1 D. L. Nelson and M. M. Cox, *Lehninger Principles of Biochemistry*, W. H. Freeman and Company, New York, 5th edn, 2008.
2 R. Breslow, *Acc. Chem. Res.*, 1995, **28**, 146–153.
3 Y. Murakami, J. Kikuchi, Y. Hisaeda and O. Hayashida, *Chem. Rev.*, 1996, **96**, 721–758.
4 H. Wei and E. Wang, *Chem. Soc. Rev.*, 2013, **42**, 6060–6093.
5 X. Wang, Y. Hu and H. Wei, *Inorg. Chem. Front.*, 2016, **3**, 41–60.
6 X. Wang, W. Guo, Y. Hu, J. Wu and H. Wei, *Nanozymes: Next Wave of Artificial Enzymes*, Springer, Berlin, 2016.
7 R. Ragg, M. N. Tahir and W. Tremel, *Eur. J. Inorg. Chem.*, 2016, **2016**, 1906–1915.
8 B. Liu and J. Liu, *Nano Res.*, 2017, **10**, 1125–1148.
9 X. Yan, *Prog. Biochem. Biophys.*, 2018, **45**, 101–104.
10 N. A. Kotov, *Science*, 2010, **330**, 188–189.
11 G. Y. Tonga, Y. Jeong, B. Duncan, T. Mizuhara, R. Mout, R. Das, S. T. Kim, Y.-C. Yeh, B. Yan, S. Hou and V. M. Rotello, *Nat. Chem.*, 2015, **7**, 597–603.
12 Q. Wang, X. Zhang, L. Huang, Z. Zhang and S. Dong, *Angew. Chem., Int. Ed.*, 2017, **56**, 16082–16085.
13 A. A. Vernekar, D. Sinha, S. Srivastava, P. U. Paramasivam, P. D'Silva and G. Mugesh, *Nat. Commun.*, 2014, **5**, 5301.
14 N. Singh, M. A. Savanur, S. Srivastava, P. D'Silva and G. Mugesh, *Angew. Chem., Int. Ed.*, 2017, **56**, 14267–14271.
15 S. Ghosh, P. Roy, N. Karmodak, E. D. Jemmis and G. Mugesh, *Angew. Chem., Int. Ed.*, 2018, **57**, 4510–4515.
16 F. Cao, E. Ju, C. Liu, F. Pu, J. Ren and X. Qu, *Chem. Commun.*, 2016, **52**, 5167–5170.
17 Y. Sang, Y. Huang, W. Li, J. Ren and X. Qu, *Chem. – Eur. J.*, 2018, **24**, 7259–7263.
18 Y. Song, K. Qu, C. Zhao, J. Ren and X. Qu, *Adv. Mater.*, 2010, **22**, 2206–2210.
19 H. Sun, Y. Zhou, J. Ren and X. Qu, *Angew. Chem., Int. Ed.*, 2018, **57**, 9224–9237.
20 S. Guo and S. Dong, *Chem. Soc. Rev.*, 2011, **40**, 2644–2672.
21 M. I. Kim, Y. Ye, M.-A. Woo, J. Lee and H. G. Park, *Adv. Healthcare Mater.*, 2013, **3**, 36–41.
22 Y. Guo, L. Deng, J. Li, S. Guo, E. Wang and S. Dong, *ACS Nano*, 2011, **5**, 1282–1290.
23 H. J. Sun, A. D. Zhao, N. Gao, K. Li, J. S. Ren and X. G. Qu, *Angew. Chem., Int. Ed.*, 2015, **54**, 7176–7180.
24 R. Zhao, X. Zhao and X. Gao, *Chem. – Eur. J.*, 2015, **21**, 960–964.
25 H. Wang, C. Liu, Z. Liu, J. Ren and X. Qu, *Small*, 2018, **14**, 1703710.
26 K. Fan, J. Xi, L. Fan, P. Wang, C. Zhu, Y. Tang, X. Xu, M. Liang, B. Jiang, X. Yan and L. Gao, *Nat. Commun.*, 2018, **9**, 1440.
27 Y. Hu, X. J. Gao, Y. Zhu, F. Muhammad, S. Tan, W. Cao, S. Lin, Z. Jin, X. Gao and H. Wei, *Chem. Mater.*, 2018, **30**, 6431–6439.
28 X. Liu and L. Dai, *Nat. Rev. Mater.*, 2016, **1**, 16064.
29 M. Zhou, H.-L. Wang and S. Guo, *Chem. Soc. Rev.*, 2016, **45**, 1273–1307.
30 V. Singh, D. Joung, L. Zhai, S. Das, S. I. Khondaker and S. Seal, *Prog. Mater. Sci.*, 2011, **56**, 1178–1271.
31 W. Yang, T. P. Fellinger and M. Antonietti, *J. Am. Chem. Soc.*, 2011, **133**, 206–209.
32 A. Levy-Lior, E. Shimoni, O. Schwartz, E. Gavish-Regev, D. Oron, G. Oxford, S. Weiner and L. Addadi, *Adv. Funct. Mater.*, 2010, **20**, 320–329.

33 D. Gur, Y. Politi, B. Sivan, P. Fratzl, S. Weiner and L. Addadi, *Angew. Chem., Int. Ed.*, 2013, **52**, 388–391.
34 A. Lopez and J. Liu, *ChemNanoMat*, 2017, **3**, 670–684.
35 H. Wei, B. Li, Y. Du, S. Dong and E. Wang, *Chem. Mater.*, 2007, **19**, 2987–2993.
36 L. Berti and G. A. Burley, *Nat. Nanotechnol.*, 2008, **3**, 81.